ELSEVIER

Journal of Photochemistry and Photobiology A: Chemistry 103 (1997) 45–50

Journal of PHOTOCHEMISTRY AND PHOTOBIOLOGY A:CHEMISTRY

Multiple emission of *N*-(1-anthryl)-pyridinium

Vladimir A. Kharlanov [a,b], Wolfgang Rettig [b,*], Michael I. Knyazhansky [a], Nadezhda Makarova [a]

[a] *Institute of Physical and Organic Chemistry, Rostov State University, Stachki str. 194/3, Rostov on Don, 344104, Russia*

[b] *Institute of Physical and Theoretical Chemistry, Humboldt University Berlin, Bunsenstr. 1, D-10117 Berlin, Germany*

Received 7 July 1996; accepted 5 September 1996

Abstract

The acceptor-substituted anthracene *N*-(1-anthryl)-2,4,6-trimethylpyridinium shows dual fluorescence with a precursor–successor relationship which is most prominent in the intermediate temperature range. At 77 K, only the short-wavelength band (anthracene type fluorescence originating formally from S_2) remains. The additional red-shifted fluorescence band observed at higher temperatures is of charge transfer type. A comparison of the radiative transition rates in absorption and emission suggests that structural relaxation leading to increased orbital overlap takes place in the excited state. This behaviour is unusual for a charge transfer state and is rationalized by the proposal of a bending motion (rehybridization of the nitrogen) induced by the increased electron density within the pyridinium ring.

Keywords: Absorption; Fluorescence; Multiple emission; *N*-(1-Anthryl)-pyridinium

1. Introduction

The unusual fluorescence and absorption properties of the *N*-anthryl derivative **1a** of the 2,4,6-trimethylpyridinium cation have been described previously [1]. To account for these properties, it was suggested [1] that the weak ($\epsilon \approx 9\ M^{-1}\ cm^{-1}$) long-wavelength band (shoulder at $\lambda_a^{max} \approx 465$ nm) can be attributed to electron transfer from the anthryl fragment (donor D) to the pyridinium ring (acceptor A) and the low-intensity fluorescence with the red-shifted structureless band ($\lambda_f = 526$ nm, ethanol, 295 K) is due to emission from the resulting biradicaloid state with the electronic structure $D^{\cdot +}$–$A^{\cdot}$ (Scheme 1) resembling the twisted intramolecular charge transfer (TICT) state [2–4]. The nature of the weak absorption band and the superposition of the bands of the separate fragments in the absorption spectrum are supported by the results [5] of a spectral calculation, using the CNDO/S method with configuration interaction [6], of the ground state equilibrium geometry of compound **1a**, which was separately determined by the AM1 method [7] using the AMPAC 5.0 package [8] with full optimization of all geometrical parameters. However, in order to gain more insight into the nature of the emissive state, the most important photophysical characteristics need to be determined. This work is directed towards the determination of the photophysical characteristics at ambient, low and intermediate temperatures.

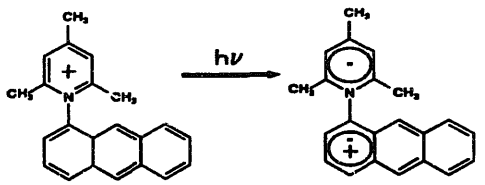

Scheme 1. Charge transfer excitation in **1a**.

2. Experimental details

2.1. Materials

Compound **1a** was prepared in the form of the perchlorate salt by known methods [9], purified by recrystallization and the product was checked for purity by fluorescence after each recrystallization step as described previously [1]. The solvent (ethanol) used was of spectroscopic grade quality (Merck, Uvasol).

2.2. Apparatus and methods

The absorption spectra were recorded with an ATI Unicam UV2 spectrophotometer (U.K.). Corrected fluorescence and

* Corresponding author. Tel.: +49 30 2093 5585; fax: +49 30 2299 535.

PII S1010-6030(96)04486-3

fluorescence excitation spectra of solutions with an absorbance $A = 0.02$–0.06 were measured with either a Perkin–Elmer 650-60 or an SLM AMINCO AB2 spectrofluorometer.

The fluorescence quantum yields ($\pm 10\%$) were determined using quinine sulphate in H_2SO_4 (0.1 N) as standard ($\Phi_f = 0.52$ [10]). Refractive index corrections were made [11] to adjust for the different solvents used.

The quantum yield changes with temperature variation were corrected with respect to the refractive index [12] and for density changes of the solvent [13].

The fluorescence lifetime measurements were performed with a single-photon counting equipment using synchrotron radiation in the single bunch mode from the Berlin storage ring BESSY as the excitation source, as described elsewhere [14]. The excitation wavelength ($\Delta\lambda = 20$ nm) was chosen at 388 nm (S_2 state, $A = 0.1$–0.4). The decay times were fitted using the iterative reconvolution procedure which allowed a time resolution down to 0.1 ns and a precision of better than 0.1 ns. Satisfactory fits ($\chi^2 < 1.2$) were obtained in all cases with one, two or three exponential terms.

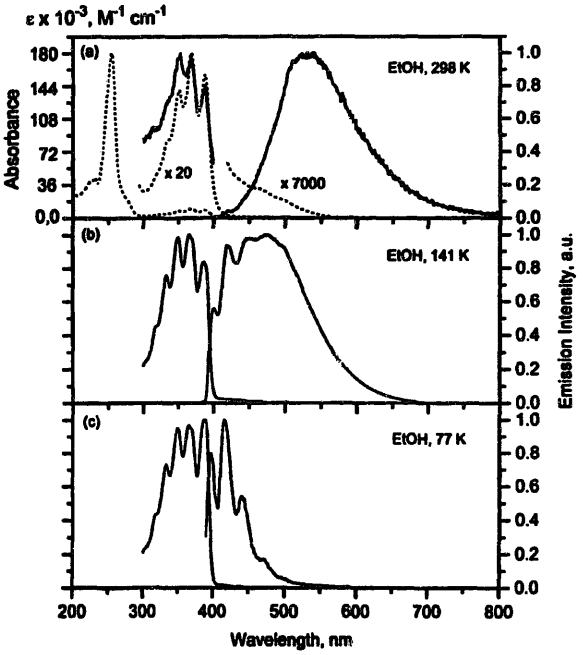

Fig. 1. Absorption and fluorescence spectra of **1a** in ethanol: (a) absorption spectrum at 298 K (– – –) and corresponding fluorescence ($\lambda_{ex} = 388$ nm) and fluorescence excitation ($\lambda_{obs} = 535$ nm) spectra (———); (b), (c) fluorescence ($\lambda_{exc} = 388$ nm) and fluorescence excitation ($\lambda_{obs} = 505$ nm and 425 nm for 141 K and 77 K respectively) spectra.

3. Results and discussion

3.1. Fluorescence at 295 K

The excitation of **1a** (ethanol, 295 K) within the S_2 absorption band at 388 nm generates a low-intensity ($\Phi_f = 0.036$, Table 1) fluorescence with a structureless band ($\lambda_f = 526$ nm) (Fig. 1(a)). The excitation spectrum remains unchanged at different wavelengths (490, 500, 526, 550, 600 or 650 nm) and closely resembles the S_2 absorption spectrum (Fig. 1(a)). Due to the low extinction coefficient of the charge transfer (CT) band, the fluorescence resulting from S_1 excitation is strongly disturbed and is not evaluated further here.

The fluorescence decay time τ_f of **1a** is nearly monoexponential, and the main component is practically invariant

Table 1
Fluorescence quantum yield (Φ_f), decay time (τ_f), radiative lifetime determined from fluorescence (τ_r) and integrated absorption (τ_r^{abs}) [a] and radiative (k_r) and non-radiative (k_{nr}) rates of *N*-anthryl-pyridinium (**1a**) (ethanol) and anthracene (ANTH) (ethanol) [11] at different temperatures

Fluorescence parameter	**1a** [b]			ANTH [11]	
	295 K	142 K	77 K	295 K	77 K
Φ_f	0.033	0.67	–	0.30	0.27
τ_f (ns)	2.6 [c]	10 [d]	13.6	5.5	6.2
τ_r (ns)	79	–	–	18.3	23.0
τ_r^{abs}(ET) [e] (ns)	4000–40 000 [f]	–	–	–	–
τ_r^{abs}(ANTH) [g] (ns)	8.86 [h]	–	–	7.82 [i], 12.8 [j], 17.9 [k]	–
k_r (10^{-7} s^{-1})	1.3	–	–	5.5	4.4
k_{nr} (10^{-7} s^{-1})	37.2	–	–	12.7	11.8

[a] Using the equations $\tau_r = \tau_f/\Phi_f$ and $1/\tau_r^{abs} = 2.88 \times 10^{-9} \nu^2 n^2 \epsilon^{max} \Delta\nu_{0.5}$ [11].
[b] S_2 excitation (388 nm).
[c] Main component (see Table 2).
[d] Strongly wavelength dependent (see Table 2); main decay component in the long-wavelength region given.
[e] Calculated from the ET absorption band of **1a**.
[f] Using $\Delta\nu_{0.5} = 1000$–$10\,000$ cm^{-1} (assumed width of the shoulder), $\epsilon^{max} = 9$ M^{-1} cm^{-1} (exp.) [1], $\nu = 21\,500$ cm^{-1} (exp.) [1] and $n = 1.3611$ for the ET absorption band [15].
[g] Calculated from the anthracene-type absorption band of **1a**.
[h] Using $\Delta\nu_{0.5} = 4500$ cm^{-1} (exp.), $\epsilon^{max} = 6390$ M^{-1} cm^{-1} (exp.) [1], $\nu = 27\,120$ cm^{-1} (exp.) [1] and $n = 1.3611$ [15].
[i] Using $\Delta\nu_{0.5} = 3500$ cm^{-1} (exp.), $\epsilon^{max} = 8500$ M^{-1} cm^{-1} (exp.), $\nu = 28\,100$ cm^{-1} (exp.) and $n = 1.3611$ [15].
[j] Berlman [16] using the equation of Strickler and Berg [17].
[k] Birks [11] (table 4.1) using the equation of Strickler and Berg [17].

Table 2
Wavelength dependence of the fluorescence decay parameters of **1a** in ethanol at various temperatures

T (K)	λ_{exc} (nm)	Fitting parameters	λ_{obs} (nm)						
			400	420	450	475	500	525	560
296	388	τ_1 (ns) (A_1)	–	–	–	–	2.6 (0.928)	2.6 (0.947)	2.7 (0.971)
		τ_2 (ns) (A_2) [a]	–	–	–	–	5.6 (0.072)	5.9 (0.053)	8.6 (0.029)
142	388	τ_1 (ns) (A_1)	1.0 (0.54)	1.0 (0.43)	1.0 (0.42)	1.2 (0.23)	–	1.4 (−0.19)	1.4 (−0.33)
		τ_2 (ns) (A_2)	2.9 (0.33)	2.8 (0.41)	3.4 (0.44)	4.1 (0.44)	6.5 (0.22)	–	–
		τ_3 (ns) (A_3)	6.2 (0.13)	6.5 (0.17)	8.6 (0.14)	9.0 (0.33)	10.5 (0.32)	9.6 (0.81)	9.9 (0.67)
77	388	τ (ns) (A)	–	13.3 (1.000)	13.8 (1.000)	–	13.8 (1.000)	–	–

[a] The nature of this second component is not clear. In view of the small fluorescence quantum yield and the small A factor, the values are less precise, and could derive from a minor impurity.

(2.6±0.05 ns) in the range (500–560 nm) of the emission band (Table 1 and Table 2, Fig. 2(a)). The radiative lifetime ($\tau_r = \tau_f/\Phi_f = 79$ ns, Table 1) differs dramatically from the radiative lifetime ($\tau_r^{abs} \approx 4000$–40 000 ns) estimated from the integrated absorption intensity and an assumed half-width ($\Delta\nu_{0.5} = 1000$–10 000 cm^{-1}) of the longest wavelength band (CT). The strong difference between the values of τ_r^{abs} and τ_r points to a change in the value of the S_1 transition moment between the absorption and the emission process. The absorption process leading to the biradicaloid structure of the Franck–Condon S_1 state is a strongly forbidden transition, which is polarized along the bond axis connecting the donor and acceptor fragments of the cation **1a** [1,5]. The emission is a weakly allowed transition and probably derives from a geometry different from the equilibrium geometry of the S_0 state. By analogy with the bent equilibrium geometry of the related CT state of the *N*-phenyl-pyridinium cation, as derived from AM1 calculations [18], it may be suggested that the S_1 excited state of *N*-anthryl-pyridinium **1a** has a similar nature; its geometry is characterized by a near sp^3 hybridization of the pyridinium nitrogen atom and a short distance between the moieties. The assumed geometry (without the methyl groups) is indicated in Fig. 6 (see Section 4).

3.2. Fluorescence at 142 K

At the intermediate temperature of 142 K, the fluorescence of **1a** becomes dual. Excitation into the S_2 state (388 nm), where the transition is localized on the anthryl fragment [1,5], leads to an emission with high quantum yield ($\Phi_f = 0.67$, Table 1) and vibrational structure at the short-wavelength edge of the fluorescence band (Fig. 1(b)). As the sharp maximum of this fluorescence resembles the typical band of anthracene (Table 3), it can be assumed that this emission represents a superposition of the long-wavelength CT band ($\lambda_f \sim 505$ nm) and a shorter wavelength locally excited (LE) fluorescence band ($\lambda_{00} \sim 397$ nm) localized on the anthryl fragment. The excitation spectra of both bands match the S_2 absorption band and establish a common precursor. The presence of two emission bands on excitation into the S_2 state is confirmed by time-resolved fluorescence which reveals different components of the fluorescence decay curves (Fig. 2(b), Table 2). In the short-wavelength range of the fluorescence spectrum (400–500 nm), the decay curves can be fitted to a sum of three exponential terms (1.0–1.2 ns, 2.9–4.1 ns and 6.2–9.0 ns components) and, in the long-wavelength range (525–560 nm), one decay (10 ns) and one rise time (1.4 ns) are sufficient. This rise component

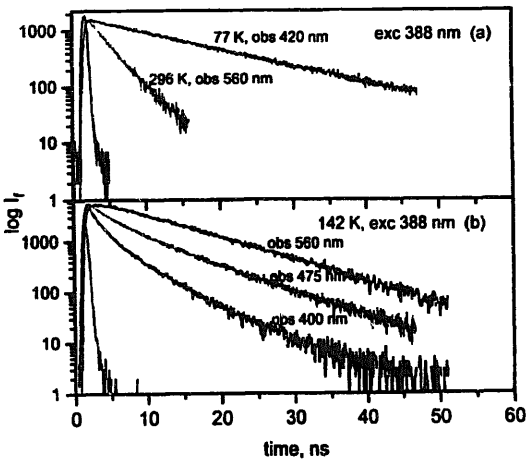

Fig. 2. Fluorescence decay curves of **1a** in ethanol ((a) at 296 K and 77 K and (b) at 142 K), observed at different wavelengths within the fluorescence spectrum. The instrument response function is also given.

Table 3
Vibrational structure in nanometres (wavenumber difference to ν_{00} (cm^{-1}) in parentheses) of fluorescence and fluorescence excitation for **1a** (ethanol, 77 K) and of fluorescence (light petroleum, 295 K) for ANTH [11]

	1a	ANTH
Fluorescence excitation	–	309 (+5695)
	333 (+4257)	323 (+4293)
	350 (+2798)	339 (+2832)
	366 (+1549)	356 (+1423)
	388 (λ_{00})	375 (λ_{00}) [a]
Fluorescence	397 (λ_{00})	377 (λ_{00}) [b]
	417 (−1208)	399 (−1522)
	441 (−2513)	423 (−2884)
	471 (−3958)	448 (−4204)
	502 (−5269)	–

[a] The data of the absorption spectrum (hexane, 295 K) were taken from Ref. [19].
[b] From Ref. [11].

approximately corresponds to the faster decay time of the short-wavelength fluorescence and suggests a parent–daughter kinetic relationship LE→CT.

3.3. Fluorescence in the intermediate temperature range

On excitation into the S_2 state (388 nm), the long-wavelength emission experiences only a weak increase in intensity on cooling from 295 K to 190 K without an essential change in the fluorescence band shape (Fig. 3 and Fig. 4(a)). On cooling further, the emission intensity and fluorescence quantum yield (Fig. 4(a)) increase more rapidly. A vibrational structure starts to develop at the short-wavelength edge, and the emission exhibits a blue shift (Fig. 4(a)).

The two very different temperature ranges of the spectral and quantum yield changes (HT, high-temperature region (295–190 K); LT, low-temperature region (less than 190 K)) may be associated with the fact that, in each range, the emission derives mainly from different states. In the high-temperature region, the CT state (A state) is the main emissive state, and in the low-temperature region, LE fluorescence (from state B) is predominant, with some contribution of CT. With decreasing temperature, an activation barrier may become active separating the two emissive states.

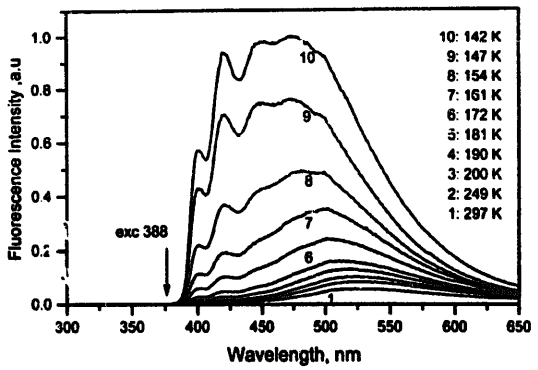

Fig. 3. Dual fluorescence of **1a** in ethanol at different temperatures.

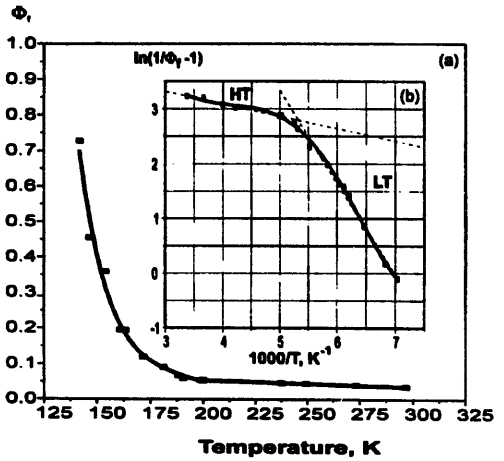

Fig. 4. (a) Temperature dependence of the overall fluorescence quantum yield of **1a** in ethanol. (b) Arrenius-type plot of the data with regression lines. HT and LT denote high- and low-temperature regions.

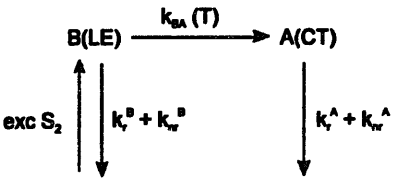

Scheme 2.

In view of the dual nature of the observed emission, the temperature dependence of Φ_f must be interpreted as the sum of the individual emission yields Φ_f^B and Φ_f^A. Assuming, as the simplest approach, a two-state irreversible mechanism (Scheme 2) with only one temperature-dependent rate constant, that of interconversion of B into A ($k_{BA}(T)$), Eqs. (1a) and (1b) can be derived for the individual fluorescence quantum yields.

$$\Phi_f^B = \frac{k_r^B}{k_r^B + k_{nr}^B + k_{BA}(T)} \tag{1a}$$

$$\Phi_f^A = \frac{k_{BA}(T)}{k_r^B + k_{nr}^B + k_{BA}(T)} \cdot \frac{k_r^A}{k_r^A + k_{nr}^A} \tag{1b}$$

In the high-temperature region, emission from B can be neglected because $k_{BA}(T) \gg k_f^B + k_{nr}^B$. The first factor in Eq. (1) is then essentially unity, and the fluorescence parameters of **1a** at room temperature (Table 1) can be interpreted as those of the A(CT) state. The fact that Φ_f depends very little on temperature in the high-temperature region (Fig. 4(a)) supports our assumption that k_{nr}^A is approximately temperature independent. In fact, the high-temperature Arrhenius activation energy is only 1.8 kJ mol^{-1}.

In the intermediate temperature region, the dual fluorescence has been interpreted by the sum of Eqs. (1a) and (1b), but for the lower part of the low-temperature range, where $\Phi_f^B \gg \Phi_f^A$, we can approximately use Eq. (1) alone. Assuming an Arrhenius activated process for $k_{BA}(T)$ (Eq. (2)), the activation energy E_{BA} separating the B(LE) and A(CT) states can be determined from the slope of a plot of $\ln(\Phi_f^{-1})$ vs. $1/T$ (Fig. 4(b)) according to Eq. (3) and Eq. (4), where E_a^{exp} is determined from the observed Arrhenius slope, if $k_{nr}^B \ll k_{BA}(T)$. The value of E_a^{exp} thus obtained in the low-temperature region is 15.6±0.7 kJ mol^{-1}.

$$k_{BA}(T) = A \exp\left(-\frac{E_{AB}}{RT}\right) \tag{2}$$

$$\ln\left(\frac{1}{\Phi_f} - 1\right)\Big|_{LT} = \ln\left(\frac{1}{\Phi_f^B} - 1\right) = \ln(k_{BA}(T) + \ln k_r^B) - \ln k_{nr}^B \tag{3}$$

$$E_a^{exp} = E_{BA} \tag{4}$$

3.4. Fluorescence at 77 K

The fluorescence at 77 K on S_2 excitation (388 nm) is further blue shifted and strong ($\Phi_f > 0.67$), and possesses a clear vibrational structure ($\lambda_{00} = 397$ nm) (Fig. 1(c)),

which is characteristic of anthracene but red shifted (Table 3). It possesses mirror symmetry and a small Stokes shift (about 580 cm^{-1}) with respect to the 00 transition of the S_2 absorption band. The fluorescence lifetime is increased and is wavelength independent in the range 420–500 nm ($\tau_f = 13.6 \pm 0.3$ ns) (Fig. 2(a), Table 2); it is similar to the radiative lifetime of anthracene at 77 K (23.0 ns [11]). Both results indicate that the emission at 77 K derives only from the LE(S_2) state. At 77 K, the transition from the B(LE) state to the CT state does not occur, probably due to the effect of the activation barrier at this low temperature. In an analogous manner, rigid media affect the fluorescence even at room temperature. In a polymer matrix (poly(methyl methacrylate) (PMMA), 295 K), the luminescence spectrum of compound **1a** exhibits only a structured band ($\lambda_{00} = 397$ nm) [1]. This lends support to the interpretation that the observed activation energy results from large-amplitude motions which are stopped in both glassy solvents at low temperature and in rigid polymers at room temperature.

4. Conclusions

The data resulting from the investigation of the excited states of the *N*-anthryl-pyridinium cation **1a** can be described within a qualitative model comprising an excited state relaxation process (Fig. 5), the nature of which is suggested by quantum chemical calculations on smaller model systems (e.g. *N*-phenyl-pyridinium ion) which allow full excited state optimization [18].

Two different characteristic geometries of the cation are possible in the lowest excited state. The first (A_{BR} in Fig. 5) possesses about the same nuclear arrangement as the geometry of **1a** in the ground state with an orthogonally twisted ($\alpha \approx 90°$ [5]) and unbent ($\beta = 180°$) conformation. For this geometry, the electronic structure is of a biradicaloid (CT) nature $D^{\cdot+}$–$A^{\cdot}$, due to the decoupled donor and acceptor orbitals, and optical transition from or to the ground state is strongly forbidden ($\tau_r > 4000$ ns) in accordance with the low extinction coefficient of the absorption band. We call this state the biradicaloid state (A_{BR}). It may correspond to an energy minimum (Fig. 5(b)) or to a Franck–Condon state (Fig. 5(a)).

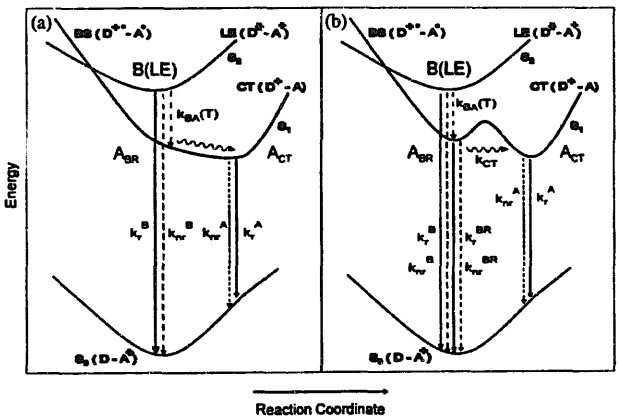

Fig. 5. Schematic potential energy scheme for the dual fluorescence of **1a** (D, anthryl fragment; A^+, pyridinium ring). Excitation into S_2 can either yield anthracene-type fluorescence (k_r^B) or internal conversion ($k_{BA}(T)$), probably via the crossing point of S_1 and S_2, leading to S_1. At the biradicaloid geometry (A_{BR}), the radiative transition rate from S_1 (k_r^{BR}) is negligibly small, but increases in intensity after structural relaxation to A_{CT} (→), from where long-wavelength fluorescence occurs (k_r^A). This structural relaxation can either be barrierless (a) or connected with an activation barrier (b). Likewise, internal conversion ($k_{BA}(T)$) is thought to be connected with an activation barrier. Radiative transitions are indicated by arrows, non-radiative transitions by broken arrows.

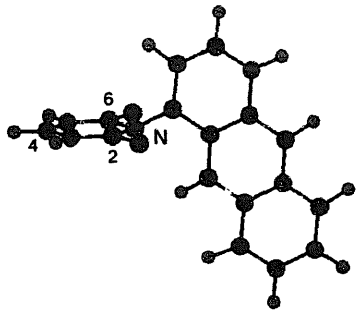

Fig. 6. The suggested relaxed excited state geometry of the *N*-anthryl-pyridinium cation **1a** explaining the weakly allowed emissive properties (approximately 7 ns) and the red-shifted emission spectrum. For simplicity, the methyl group in position 4 of the pyridinium ring and the hydrogen atoms of the methyl groups in positions 2 and 6 are not shown.

The overall minimum in S_1 (A_{CT} in Fig. 5) corresponds to an arrangement which is still orthogonal, but bent ($\beta > 180°$, Fig. 6), and leads to a weakly allowed CT emission (526 nm, $\tau_r \approx 79$ ns). The increased transition moment for this transition can be attributed to the interaction between the highest occupied molecular orbital (HOMO) localized on the anthryl fragment (donor) and the lowest unoccupied molecular orbital (LUMO) localized on the pyridinium ring (acceptor) due to geometric distortion (bending, Fig. 6). Because the distorted geometry can be reached by relaxation in the excited state, we call this state the relaxed CT state (A_{CT}).

In liquid medium (ethanol, 298 K), excitation into the S_2 state (B(LE), 388 nm) leads to emission from the A_{CT} state and therefore involves, within this model, a bending motion along the reaction coordinate.

In rigid medium (ethanol, 77 K; PMMA, 298 K), the relaxation from the B(LE) state to the A_{CT} state is strongly decreased such that only emission from the B(LE) state is observed. A probable explanation for this behaviour is that high-viscosity conditions render the large-amplitude excited state relaxation (bending), leading from the B(LE) to the A_{CT} state, more difficult.

At intermediate temperatures (in the range 190–142 K), the possibility for the population of both radiative states and for the observation of dual fluorescence arises, with a mixture of the A_{CT} fluorescence band (526 nm) and the B(LE) fluorescence band (397 nm). Our experimental data are consistent with both potential energy schemes: the simple scheme in Fig. 5(a), where the relaxation of B(LE) occurs directly to A_{CT} without activation energy in the S_1 state, and that in

Fig. 5(b), where relaxation involves passage through the biradicaloid structure A_{BR} and where an additional activation energy in S_1 may be involved. The effect of this barrier does not manifest itself as long as $k_{CT} \gg k_{nr}^{BR}$.

Acknowledgements

The support by the Volkswagen Stiftung is gratefully acknowledged.

References

[1] V.A. Kharlanov, M.I. Knyazhansky, N.I. Makarova and V.A. Lokshin, *J. Photochem. Photobiol. A: Chem., 70* (1993) 223.
[2] Z.R. Grabowski, K. Rotkiewicz, A. Siemiarczuk, D.J. Cowley and W. Baumann, *Nouv. J. Chim., 3* (1979) 443.
[3] W. Rettig, *Angew. Chem., 98* (1986) 969; *Angew. Chem. Int. Ed. Engl., 25* (1986) 971.
[4] W. Rettig, *Top. Curr. Chem., 169* (1994) 254.
[5] V.A. Kharlanov, M.I. Knyazhansky and W. Rettig, *J. Mol. Struct., 380* (1996) 113.
[6] J. Del Bene and H.H. Jaffe, *J. Phys. Chem., 48* (1968) 1807; *48* (1968) 4050; *49* (1968) 1221; *50* (1969) 1126. H.M. Chang, H.H. Jaffe and C.A. Masmanidis, *J. Chem. Phys., 79* (1975) 1109, 1118. J. Del Bene, *J. Am. Chem. Soc., 95* (1973) 6517; *J. Chem. Phys., 62* (1975) 666; *J. Chem. Phys., 62* (1975) 1961.
[7] M.J.S. Dewar, E.G. Zoebisch, E.F. Healy and J.J.P. Stewart, *J. Am. Chem. Soc., 107* (1985) 3202.
[8] M.J.S. Dewar, J.J.P. Stewart, J.M. Ruiz, D. Liotard, E.F. Healy and R.D. Dennington II, *AMPAC 4.5 and AMPAC 5.0*, Semichem., Shawnee, 1993 and 1994.
[9] A.T. Balaban, A. Dinculescu, F. Iordache, F. Chiralen and D. Patsioia, *Chem. Scr., 18* (1981) 230.
[10] S.R. Meech and D. Phillips, *J. Photochem., 23* (1983) 193.
[11] J.B. Birks, *Photophysics of Aromatic Molecules*, Wiley-Interscience, 1970, Table 3.1.
[12] J.A. Riddick and W.B. Bunger, *Organic Solvents*, Wiley-Interscience, New York, 1980.
[13] R. Passerini and J.G. Ross, *J. Sci. Instrum., 30* (1953) 274–279.
[14] M. Vogel and W. Rettig, *Ber. Bunsenges Phys. Chem., 91* (1987) 1241.
[15] D.R. Lide (ed.), *CRC Handbook of Chemistry and Physics*, CRC Press, Boca Raton, 73rd edn., 1992.
[16] I.B. Berlman, *Handbook of Fluorescence Spectra of Aromatic Molecules*, Academic Press, New York, London, 2nd edn., 1971.
[17] S.I. Strickler and R.A. Berg, *J. Chem. Phys., 37* (1962) 814.
[18] V.A. Kharlanov and W. Rettig, unpublished results, 1996.
[19] E.S. Stern and C.I. Timmons, *Electronic Absorption Spectroscopy in Organic Chemistry*, Edward Arnold, London, 1970, Chapter 6, Table 6.4.